ORIGINAL RESEARCH (AR) DOI: 10.4274/jems.2024.79027

Journal of ETA Maritime Science 2024;12(3):346-356

Parameter Optimization for Model-Based Design and Control of the KVLCC2 Tanker Ship

Emre Sayin, Ismail Bayezit

İstanbul Technical University Faculty of Aeronautics and Astronautics, Department of Aeronautical Engineering, İstanbul, Türkiye

Abstract

This article provides a model-based design method for heading control based autonomous trajectory tracking of a KVLCC2 ship. Kinematics, dynamics, and hydrodynamic force subsystems are used to represent the ship's motion equations. By contrasting the outcomes with experimental data received from the maneuvering modelling group, the accuracy of the model is confirmed. Heading angle of the ship is controlled by a linear cascade controller, and the settings of the controller are modified by using two separate heuristic optimization techniques: particle swarm optimization and genetic algorithm. The comparison of the findings demonstrates that the particle swarm optimization approach is computationally more effective than the genetic algorithm. Performance in the presence of disturbance has been investigated using the controller parameters discovered using particle swarm optimization. A suitable guidance algorithm is incorporated into the architecture of a trajectory tracking system to establish the necessary heading angle for travel between waypoints. We use a real-time simulator to visualize the ship motion on a graphical environment.

Keywords: Ship heading control, Cascade control, Model-based simulation, Genetic algorithm, Particle swarm optimization

1. Introduction

In the ever-evolving landscape of maritime transportation, the efficient and precise control of vessels remains a pivotal challenge. The utilization of modern control strategies, grounded in model-based design, presents an avenue of exploration to enhance the performance of vessels like the KVLCC2 tanker. The central focus of this study revolves around the implementation and advantages of cascade control approach and optimization of controller parameters, a crucial facet in achieving optimal control outcomes. Leveraging the innovative paradigms of particle swarm optimization (PSO) and genetic algorithms (GAs), this research delves into the synergy between advanced control methodologies and state-of-the-art optimization techniques. By combining the principles of model-based control, cascade control architecture, and the potency of optimization, this study offers insights into the broader realm of complex systems optimization as well as contributing to the emerging field of the maritime control engineering.

By analyzing the system dynamics, it is possible to design a controller that can transform a manually controlled system into an autonomously controlled one. Most control systems are closed-loop systems that use feedback from the system's output to generate an error signal, which is then compensated by using a controller to implement certain algorithms.

Scope of this work is the simulation of the dynamics of the ship motion, design and implementation of a linear cascade controller within the model-based design and simulation environment, and to satisfy the autonomous heading tracking performance. The control methodology for the system is chosen as in the cascade control scheme using a deterministic approach. This control method involves the utilization of various control loops, in which, each loop is responsible for controlling a specific aspect of the system's behaviour. The output of one control loop is used as the input to the next control loop, resulting in a hierarchical control structure that can be finely tuned to achieve the desired system behaviour. The aforementioned control

Address for Correspondence: Ismail Bayezit, İstanbul Technical University Faculty of Aeronautics and Astronautics, Department of Aeronautical Engineering, İstanbul, Türkiye
E-mail: bayezit@itu.edu.tr
ORCID iD: orcid.org/0000-0001-9345-5108

Received: 30.04.2024
Last Revision Received: 07.08.2024
Accepted: 11.08.2024

To cite this article: E. Sayın, and İ. Bayezit. "Parameter Optimization for Model-Based Design and Control of the KVLCC2 Tanker Ship". *Journal of ETA Maritime Science*, vol. 12(3), pp. 346-356, 2024.

algorithm also allows the fast rejection of disturbance since one loop perceive the disturbance prior to other loop and obtains chance to compensate the disturbance before it propagates [1]. Cascade control is commonly used in complex systems where a single control loop may not be sufficient to achieve the desired level of performance. Several studies have been done on the ship heading control by using cascade approach. In [2], Kula designs a heading control system by using a cascade system and internal model control approach. Li and Wang [3] propose a hybrid approach for ship dynamic positioning control that uses piecewise and cascade controllers. However, they do not make any tuning of controller parameters [3]. Tao and Ma [4] design a robotic arm for steering wheel control of the ship. They use as cascade approach to control the steering angle with PID controllers. They do not utilize any tuning of the PID parameters [4]. Zhibin et al. [5] design a cascade controller for an autonomous underwater vehicle. They use PI and P controllers for inner and outer loops, respectively. They optimize the controller parameters. However, the optimization method used for tuning the controller parameters is not shared [5]. Andrija et al. [6] manufacture an unmanned surface vehicle and use PID controllers to control throttle and steering of the ship. They tune controller parameters manually [6]. Many other advanced control algorithms have been presented for ship control such as LQR [7] MPC [8-10] neural network-based controllers [11,12] sliding mode controller [13-15], non-linear adaptive control [16] and so on.

Additionally, studies on the path following of KVLCC2 tanker are also abundant. Paramesh and Rajendran investigate the PID controlled KVLCC2 tanker for heading control. They use a Line-of-Sight (LOS) guidance algorithm to navigate between given waypoints [17]. Adams et al. [18] proposes an MPC, PID and LQR based heading control of KVLCC2 tanker. They also use LOS guidance algorithm and compare the performances of controllers [18]. Sandeepkumar et al. [19] design a non-linear MPC for the KVLCC2 tanker. They develop a 3 DoF Maneuvering model and design an MPC to control the heading angle in the presence of regular waves [19]. Wang et al. [20] develops a control approach using Deep Reinforcement Learning technique in order to execute the path following of 7 meters scaled version of KVLCC2 tanker ship. They use Adaptive LOS guidance method to convert waypoints into heading angle commands. Different controller methods are also compared in the study [20].

The rest of this paper is organized as follows: In the second chapter, the equations of motion that are essential for the development of the model are discussed and validated. In the third chapter, the control strategy used to regulate the ship's heading angle is described in detail, including the application of optimization methods for controller parameter tuning and comparison of these tuning techniques. The fourth chapter focuses on the implementation of a path tracking system and real-time simulation. Lastly, in the fifth chapter, the study has been concluded and strategies for future research are proposed.

2. Equations of Motion

The coordinate systems used to analyze the ship motion is given in Figure 1. The three degrees-of-freedom (DoF) motion of a ship (including yaw, surge, and sway) can be given using differential relations. The non-linear equations of motion for a ship with these three DoF can be written as follows [21]:

$$\begin{bmatrix} m+m_x & 0 & 0 \\ 0 & m+m_y & x_G m \\ 0 & x_G m & I_{zG}+x_G^2 m+J_z \end{bmatrix} \begin{bmatrix} \dot{u} \\ \dot{v}_m \\ \dot{r} \end{bmatrix} = \begin{bmatrix} X+(m+m_y)v_m r+x_G m r^2 \\ Y-(m+m_x)ur \\ N_m-x_G mur \end{bmatrix} \quad (1)$$

u and v_m are the surge and lateral velocities at the center of the ship, respectively. r is the yaw rate, m is the ship mass, m_x and m_y are the added masses for x and y axis directions. $\boldsymbol{x}_G$ is the longitudinal coordinate value of the of gravity (CoG) of the ship, I_{zG} is the ship moment of inertia calculated around CoG and J_z is the added moment of inertia. X and Y stand for surge and sway forces. N_m is the yaw moment calculated around the center of the ship excluding added mass term. This information is useful for having insight into the ship behaviour for designing control strategies to achieve a desired performance.

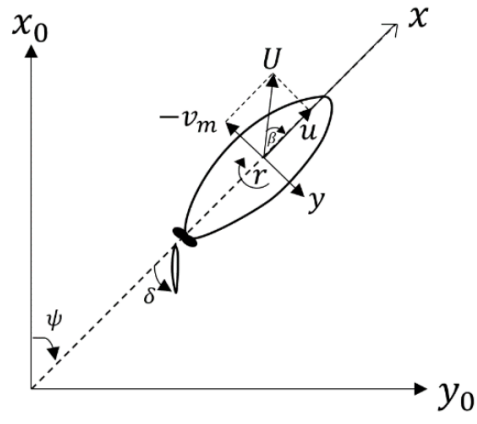

Figure 1. *Ship coordinate system*

2.1. Kinematics

The kinematics equations for a ship can be derived by using appropriate coordinate transformations. The dynamics equations, on the other hand, are typically described in a fixed-body frame, as shown in Figure 1. In this frame, the x-axis points toward the ship's bow, y-axis points toward the starboard side, and right-hand rule is used to find the z-axis,

which completes the axes. To visualize the ship motion in an inertial frame, it is necessary to convert the body-fixed coordinates into Earth-fixed inertial coordinates. The Earth-fixed inertial coordinate system has an origin fixed at the Earth's center; x-axis points toward the North, y-axis points toward the East, and the z-axis completes the right-hand rule. Both angular and linear motions of the ship must be converted into this coordinate system in order to fully describe the motion dynamics of the ship in a fixed frame of reference [22]. Proper transformations are made according to these conversions.

2.2. Hydrodynamic Forces

This section reveals the hydrodynamic forces that act on the ship as: forces that act on ship hull (H), forces due to propeller (P) and forces by steering (R). It is obvious that adding extra forces into these equations is possible for ongoing advanced studies. The forces acting on a ship can be elaborated as:

$$\begin{aligned} X &= X_H + X_R + X_P \\ N_m &= N_H + N_R \\ Y &= Y_H + Y_R \end{aligned} \tag{2}$$

where X_H and Y_H are surge and sway forces; N_H is the yaw moment calculated around the center of the ship acting on ship hull, excluding the added mass components, respectively. X_R and Y_R are surge and sway forces and N_R is the yaw moment around midship by steering. X_P represents the propeller-induced surge force. These forces are completed by using set of equations and hydrodynamic derivatives obtained experimentally.

Hydrodynamics forces acting on a ship hull can be elaborated by set of equations. For the surge, sway, and yaw motions, the forces that act on ship hull can be calculated as [21]:

$$\begin{aligned} X_H(v_m, r) &= -R_0 + X_{vv}v_m^2 + X_{vr}v_m r + X_{rr}r^2 + X_{vvvv}v_m^4 \\ Y_H(v_m, r) &= Y_v v_m + Y_R r + Y_{vvv}v_m^3 + Y_{vvr}v_m^2 r + Y_{vrr}v_m r^2 + Y_{rrr}r^3 \\ N_H(v_m, r) &= N_v v_m + N_R r + N_{vvv}v_m^3 + N_{vvr}v_m^2 r + N_{vrr}v_m r^2 + N_{rrr}r^3 \end{aligned} \tag{3}$$

where R_0 is the resistance coefficient, N_v, N_R, N_{vvv}, N_{vvr}, N_{vrr}, N_{rrr}, X_{vv}, X_{vr}, X_{rr}, X_{vvvv}, Y_v, Y_R, Y_{vvv}, Y_{vvr}, Y_{vrr}, and Y_{rrr} are the hydrodynamic derivatives on maneuvering. These coefficients can be determined both computationally by using CFD tools and experimentally. Bold usage indicates the non-dimensional form. The dimensionalized form of the coefficients X_H, Y_H, and N_H can be written as:

$$\begin{aligned} X_H &= 0.5\rho\, L_{pp} d U^2 X_H \\ Y_H &= 0.5\rho\, L_{pp} d U^2 Y_H \\ N_H &= 0.5\rho\, L_{pp}^2 d U^2 N_H \end{aligned} \tag{4}$$

where ρ, L_{pp}, d and U are the density of water, ship length, ship draft and resultant speed, respectively. Additionally, $\boldsymbol{v_m}$ and $\boldsymbol{r}$ can be found by calculating v_m/U and rL_{pp}/U, respectively.

It is assumed that the hydrodynamic force arisen from the propeller is only affecting surge movement of the ship. Thus, a surge force X_P is produced by propeller. X_P can be calculated as:

$$X_P = (1 - t_p)T \tag{5}$$

t_p is the thrust deduction factor and T is the thrust of the propeller, which can be calculated as given in [1] and [2]:

$$T = \rho n_p^2 D_p^4 K_T(J_P) \tag{6}$$

where n_p is the revolution number and D_p is the diameter value of the propeller, respectively. K_T is a 2nd order polynomial that is a function of propeller advanced ratio J_P, and can be calculated as:

$$K_T(J_P) = k_2 J_P^2 + k_1 J_P + k_0 \tag{7}$$

where $k\,0$, k_1 and k_2 are the elements of K_T polynomial. Additionally, J_p can be calculated as:

$$J_p = \frac{u(1-w_p)}{n_p D_p} \tag{8}$$

where w_p is the wake coefficient at propeller position during maneuvering, which is calculated as:

$$w_p = 1 - (1 - w_{p0})\left(1 + \left(1 - e^{-C_1|\beta_p|}\right)(C_2 - 1)\right) \tag{9}$$

w_{p0} is the propeller position wake coefficient during straight motion, β_p is the geometrical inflow angle to propeller for maneuvering motions, C_1 and C_2 are the experimental constants that stand for wake characteristics in maneuvering.

Due to presence of rudder, there also exists a hydrodynamic force acting on surge, sway and yaw motions. Hydrodynamic forces by steering can be formulated as [3]:

$$\begin{aligned} X_R &= -(1 - t_R)F_N \sin\delta \\ Y_R &= -(1 + a_H)F_N \cos\delta \\ N_R &= -(x_R + a_H x_H)F_N \cos\delta \end{aligned} \tag{10}$$

where F_N and $t\,R$ are the normal force of the rudder and the steering resistance deduction factor, respectively. The increase factor of the rudder force, the rudder position longitudinal coordinate, the longitudinal coordinate value of acting point of the additional lateral force, and the rudder angle are given with a_H, x_R, x_H, and δ, respectively. F_N can also be calculated as:

$$F_N = 0.5\rho A_R U_R^2 f_\alpha \sin\alpha_R \tag{11}$$

where $A\,R$ is the profile area value of the movable part of mariner rudder, f_α is the lift gradient coefficient of the

rudder, α_R is the effective inflow angle to rudder and U_R is the resultant inflow velocity to the rudder. U_R can be calculated as:

$$U_R = \sqrt{(u_R^2 + v_R^2)} \tag{12}$$

where u_R is the longitudinal and v_r is the lateral inflow velocity components to rudder. Additionally, α_R can be calculated from:

$$\alpha_R = \delta - tan^{-1}\left(\frac{v_R}{u_R}\right) \tag{13}$$

v_R can be calculated from:

$$v_R = U\gamma_R\beta_R \tag{14}$$

where γ_R and β_R are the flow straightening coefficient and the effective inflow angle to rudder for maneuvering motions, respectively. β_R can be calculated as:

$$\beta_R = \beta - \boldsymbol{l_R} \tag{15}$$

where β and $\boldsymbol{l_R}$ are the hull drift angle at midship and the dimensionless effective longitudinal coordinate value of the rudder position, respectively. Additionally, u_R can be calculated from:

$$u_R = \epsilon u(1 - w_p)\sqrt{\eta\left\{1 + \kappa\left(\sqrt{1 + \frac{8K_T}{\pi J_P^2}} - 1\right)\right\}^2 + (1 - \eta)} \tag{16}$$

where, ϵ is the ratio between the wake fraction at rudder position and propeller position, w_p is the propeller position wake coefficient for maneuvering motions, η is the ratio between the diameter of the propeller and rudder span. κ is an experimental constant.

2.3. Model Validation

Validation of the model is verified by conducting turning and zig-zag maneuvering tests. Parameters of the ship used in the model are taken from 7 meters KVLCC2 model [21]. Initial surge velocity is chosen as 1.179 m/s and propeller revolution is kept constant as 11.86 rps. In the turning maneuver test, a 35 degree of rudder angle is applied to the system after 1 second of ship movement. The resulting dimensionless trajectory of the ship and experimental data taken from [21] are compared and shown in Figure 2. The dimensional trajectories for turning maneuver tests with ±35 degree rudder angles are shown in Figure 3. It is resulted that the surge velocity (u) stabilizes to a value of 0.544 m/s whereas the yaw rate (r) stabilizes to a value of 0.063 rad/s (given in Figure 4). By using the basic equation for circular motion, the standard turning diameter can be calculated to be approximately 17.27 meters, which is consistent with the trajectory shown in Figure 3. Comparison of non-dimensional turning maneuver parameters with experimental data taken from [21] are given in Table 1.

Additionally, we conducted a zig-zag maneuver test. The performed zig-zag maneuver test simulation is given in Figure 5. Comparison of zig-zag maneuver test overshoot angles (OSA) with experimental data taken from [21] is given in Table 2. These tests allowed for the assessment of the model's accuracy and the identification of any discrepancies between the simulated and actual ship behaviour.

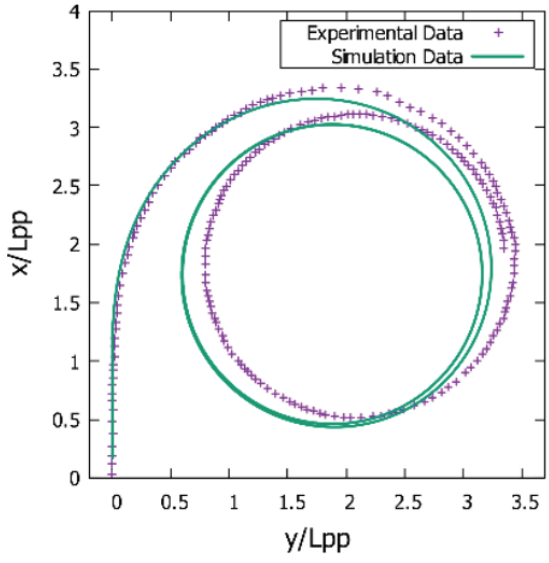

Figure 2. *Data comparison*

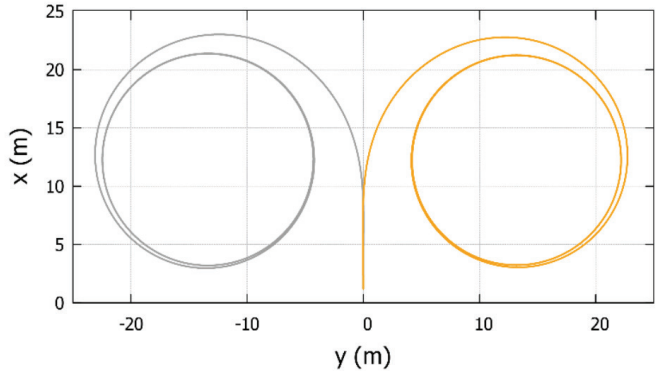

Figure 3. *±35 degree turning maneuver*

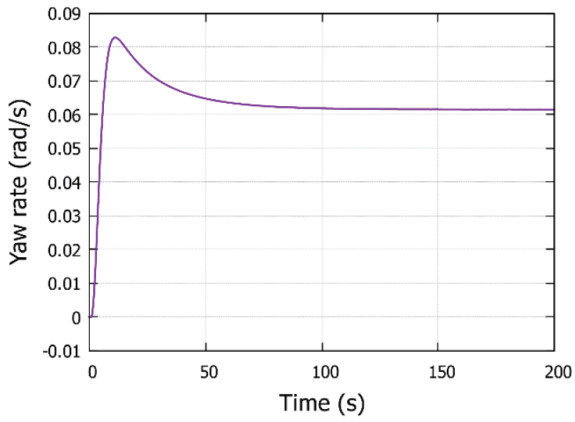

Figure 4. *Yaw rate change for turning maneuver*

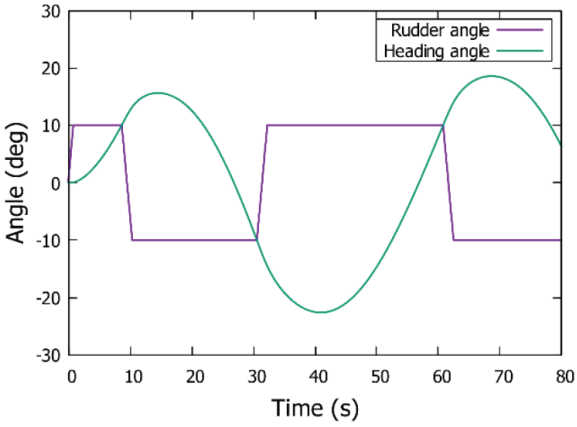

Figure 5. *Zig-zag maneuver test*

Table 1. *Turning maneuver comparison between numerical and experimental data*

Parameter	Experimental value	Simulation value	Error (%)
Advance (β = 35°)	3.25	3.19	2
Transfer (β = 35°)	1.7	1.31	23
Tactical Diameter (β = 35°)	3.34	3.18	5
Advance (β = -35°)	3.11	3.22	4
Tactical Diameter (β = -35°)	1.95	1.33	32

Table 2. *Zig-zag maneuver comparison between numerical and experimental data*

Parameter	Experimental value	Simulation value
1st OSA	8.2	5.61
2nd OSA	21.9	12.63

It is possible to extrapolate that the model accurately represents the behaviour of the ship with regards to its trajectory based upon the comparison of the simulated and experimental data. The similarity between simulated results and experimental data suggests that the

3. Control Strategy

A cascade control scheme is chosen to satisfy the heading stability of the ship. Both yaw rate and yaw angles are controlled in this approach. The outer loop stabilizes the ship's yaw angle, while the inner loop controls the yaw rate. The control structure used in system is given in Figure 6.

In the cascade control approach, it is important to ensure that the inner control loop response is faster than the outer control loop, as this allows the system to be more resistant to disturbances. It is generally recommended that the inner control loop to be at least 3 times faster than the outer control loop in order to achieve this [25]. To check this condition, two tests are conducted without controller gains. In the first test, the inner loop is closed and the outer loop is opened. A step input is applied to the inner loop, and the response of the inner loop is measured. Rise time of the inner loop is determined as 1.01 sec. In the second test, the primary loop is closed and the secondary loop is opened. A step input is applied to the outer loop, and the rise time of the outer loop is determined as 11.11 sec. It is observed that the rise time of the inner loop is approximately 11 times smaller than the rise time of the outer loop. This meets the criteria that requires for secondary loop to be at least three times faster than the primary loop in a cascade control system, as it demonstrates that the inner loop has a significantly faster response time when comparing with the outer loop. One can say that this will develop the performance of the system by allowing the inner loop to more quickly respond to changes in the outer loop output. By assuming G_{c_1} and G_{c_2} are proportional controllers which have the coefficients k_1 and k_2, the control law of the cascade system can be written as:

$$u = \mathrm{k}_2\left(k_1\left(\psi_{ref} - \psi_{out}\right) - r\right) \tag{17}$$

where u is the control input, G_{c_1} and G_{c_2} are the primary and secondary controllers, respectively. Proportional controllers are used as inner and outer loop controllers.

Controller parameters are optimized via GA and PSO techniques. The selection of the parameters is performed using an evaluation criterion known as the fitness function [26]. Different performance criteria were implemented in the literature such as Sum Absolute Error [27]. In our case, the fitness function is chosen as the Integrated Time Absolute Error (ITAE) to be minimized. It is a well-known control performance criterion with the advantages of

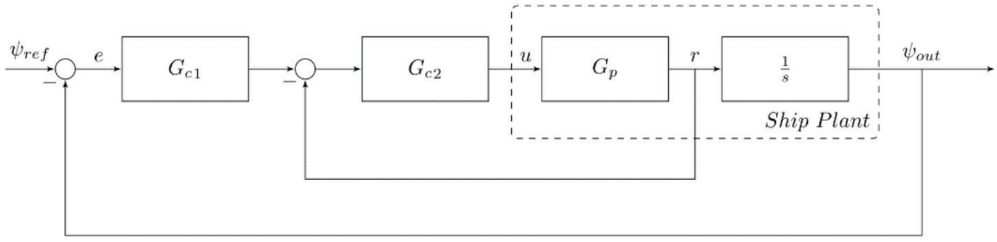

Figure 6. *Control scheme of the ship system*

obtaining smaller overshoots and oscillations than alternative performance criterions such as integral absolute error and integral square error. Mathematical representation of the ITAE can be written as [28]:

$$ITAE = \int_0^T t|e|dt \tag{18}$$

where e is the error between reference and feedback, t is the time. For the cascade loop structure, two different ITAE values obtained and added together as a single performance criterion. First ITAE value has been calculated for the difference between output heading angle and the reference heading angle whereas the second one has been calculated between the yaw rate of the ship and heading angle error multiplied by the controller. The objective function J can be written as [29]:

$$J = ITAE_1 + ITAE_2 \tag{19}$$

where $ITA\,E_1$ and $ITA\,E_2$ are obtained from the outer loop and inner loop, respectively.

3.1. GA-Based Tuning

GA is a well-known optimization technique used to find extremum value of a function. GA is inspired by the process of evolution in nature and is based on the principles of natural selection. Initial population develops as the generations pass thanks to the elimination of genetically poor individuals [30]. The GA process consists of several basic steps, including population initialization, selection, crossover, and mutation. The process is completed once the termination criterion is met. Controller parameters are k_1 for primary and k_2 for the secondary loop. Parameters of the GA function are given in Table 3.

Table 3. *Genetic algorithm implementation parameters*

Population size	50
Lower boundary	[0 0]
Upper boundary	[100 100]
Number of max. generations	500
Stop criterion	1e-3
Crossover fraction	0.8
Mutation function	Gaussian

The iteration process for GA can be explained as follows [31,32]:

1. Initialize population with random numbers for controller gains, k_1 and k_2. Members of the population are called chromosomes.
2. Calculate the function value of each chromosome.
3. Select the best chromosomes as to be having higher chance for the next generation.
4. Crossover randomly selected chromosomes.
5. Mutate the population for next generation.
6. If the stop criterion is satisfied, choose k_1 and k_2 as the best controller parameters. Otherwise, return step 2.

A signal that consists of different steps is applied to the system and objective function J is minimized by the GA algorithm. After 57 Generations, the algorithm found the minimum value of J to be 34.2854 and the optimum controller parameters for this criterion are found to be $k_1 = 0.3733$ and $k_2 = 64.6377$. Reference signal and heading angle response of the system for the 5th and optimal generations are given in Figure 7. As shown in the figure, the system evolved a behaviour with lower oscillation and overshoot, which is the expected result of the optimization process. The GA showed its efficiency to obtain the optimum system parameters to achieve the desired performance.

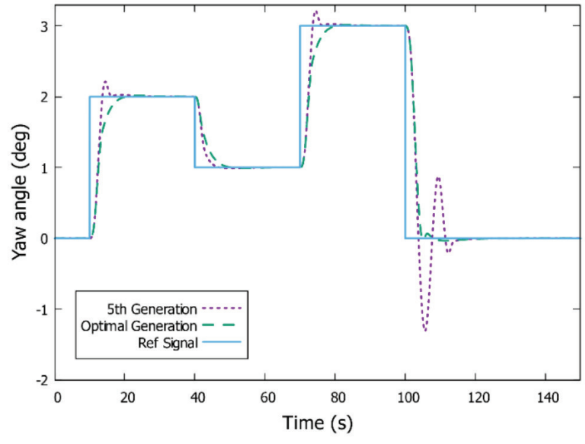

Figure 7. *Yaw angle response during different generations of GA*

GA: Genetic algorithm

3.2. PSO Based Tuning

PSO, is another nature-inspired optimization technique based on the behaviour of swarms. An initial population is set at the beginning of the algorithm that is randomly distributed in the search space. Position and velocity need to be given to every population member. During each iteration, the position and velocity of each member of the population are updated based on the best member of the population [33]. This allows the population to converge towards the optimal solution as the iterations progress.

Let us represent N possible solutions as $X = [k_1, k_2, \ldots k_N]$ whereas elements of vector $k_i = \left[k_{1_i}\ k_{2_i}\right]$ as the gains of outer and inner loops, respectively. For each step, the particles are updated according to the formula [34]:

$$x_i(t+1) = x_i(t) + v_i(t+1) \tag{20}$$

where v_i is the velocity of the particle that can be calculated from:

$$v_i(t+1) = \mathrm{w}v_i(t) + c_1\big(p_i - x_i(t)\big)R_1 + c_2\big(g - x_i(t)\big)R_2 \tag{21}$$

where p_i is the best solution for that individual particle obtained so far, g is the global best, i.e. the best solution of the swarm overall, w is the inertia weight coefficient, c_1 is cognitive coefficient and c_2 is social coefficient. These coefficients regulate the magnitudes of personal and global best solutions. R_1 and R_2 are diagonal matrices between 0 and 1 that are distributed uniformly [35].

For PSO-based optimization, the same fitness and cost functions are used given in equations (18) and (19). The significant PSO parameters are listed in Table 4. To achieve an efficient solution, a swarm size value of 80 is chosen, as suggested by [36].

Table 4. *Particle swarm optimization parameters*

Swarm size	80
Lower bound	[0 0]
Upper bound	[100 100]
Stop criterion	1e-3

The optimization process took 24 iterations to reach the optimal point. The optimum parameters are found to be $k1 = 0.3737$ and $k_2 = 66.7472$. For a reference input, responses of the 1st iteration and optimum iteration are given in Figure 8, which shows the superior performance of the optimal iteration than the first one.

Additionally, disturbance rejection performance of the system is evaluated. The wave disturbance which is a dominant disturbance for a ship can be approximated linearly as an output $y(s)$ [37]:

$$\mathrm{y(s)} = \mathrm{h(s)}\omega\mathrm{(s)} \tag{22}$$

where $\omega(s)$ is a Gaussian white noise that has zero-mean and unity power, $h(s)$ is the transfer function. For $h(s)$, a 2nd order transfer function approximation can be established:

$$\mathrm{h(s)} = \frac{2\lambda\omega_0\sigma s}{s^2+2\lambda\omega_0 s+\omega_0^2} \tag{23}$$

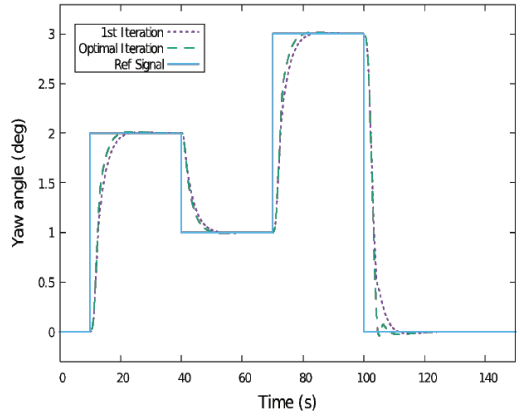

Figure 8. *Response of the PSO for different iterations*

PSO: Particle swarm optimization

where λ is the damping coefficient, σ is a constant that expresses wave density and $\omega 0$ is the dominating wave frequency.

The heading tracking behaviour of the ship is tested under different sea conditions. To mimic these conditions, wave density, σ has been changed while the other parameters, λ and ω_0 are kept constant as 0.1017 and 0.7222, respectively. The σ value has been changed as 1, 2 and 10, where the value of 10 means around maximum 40% deviation from the 1 deg. of heading angle command.

The system response under commanded reference heading signal in the presence of different wave disturbances is given in Figure 9, which demonstrates that the ship is able to track the reference input effectively despite the presence of different sea states.

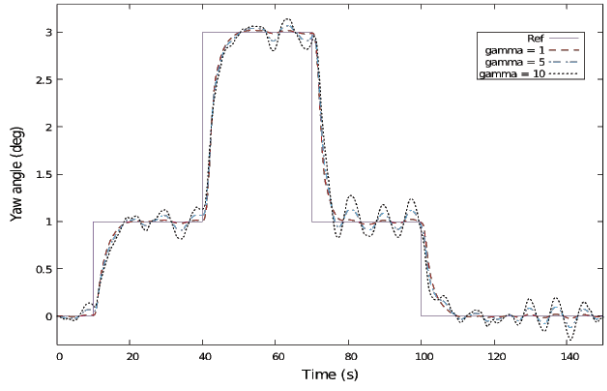

Figure 9. *Yaw angle output in the presence of disturbance*

Additionally, system response in the presence of disturbance is also evaluated for the controller parameters obtained by GA. To compare the controllers, root mean square error (RMSE) values between the output and reference angle given in Figure 9 is calculated. According to the results, RMSE value of PSO is 0.3657 whereas this value is 0.3666 for GA, which shows that PSO is slightly superior than GA in the presence of disturbance.

4. Simulation Results

4.1. Comparison of Tuning Algorithms

The computation times of both optimization algorithms, GA and PSO, are investigated. The time of computation for the GA algorithm is 47 minutes, while the time of computation for the PSO algorithm is 34 minutes. This result indicates that the PSO algorithm is approximately 1.38 times faster than the GA algorithm. Fitness function values of the algorithms during iterations are given in Figures 10 and 11. The controller parameters found by PSO algorithm have been chosen to proceed on.

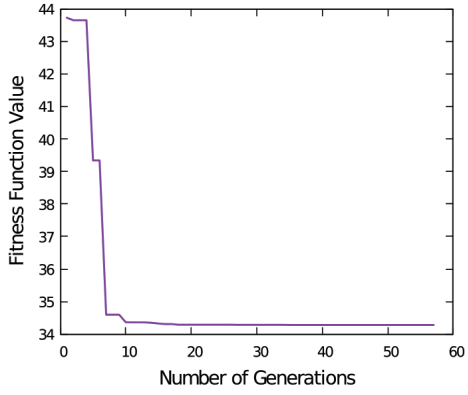

Figure 10. *Fitness function evolution for GA*

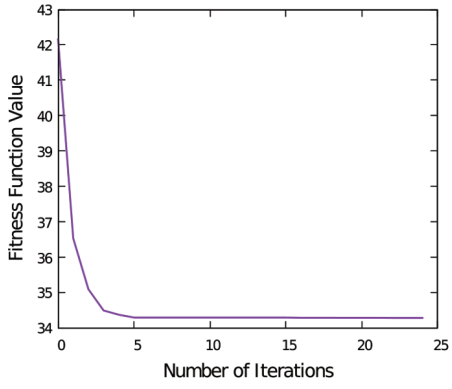

Figure 11*. Fitness function evolution for PSO*

Once the ship is able to track the given heading angle signal, it is possible to generate waypoints to determine the required path and yaw angle to navigate between points. For a given waypoint, (x, y) the required guidance equation that converts given waypoints into heading angle command, ψ_{cmd} can be written as [27,37]:

$$\psi_{cmd}(\mathrm{t}) = atan2\big(y_k - y(t), x_k - x(t)\big) \tag{24}$$

where x_k and y_k stand for the position of the next waypoint. Equation (24) is also called the LOS guidance law. The function $atan2$ is used to assure that the $atan2(y,x)$ stay between $-\pi$ and π. To test the path tracking performance of the ship, four waypoints are given as (30,20), (50,100), (60,80), (70,30) meters, respectively. Trajectory of the ship under given waypoints is given in Figure 12, which shows that the ship has the capability of following the given waypoints accurately. Additionally, rudder deflection of the ship during the waypoint tracking process is given in Figure 13.

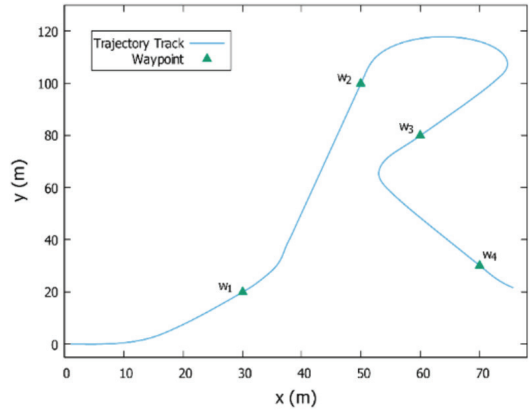

Figure 12*. Trajectory of the ship during waypoint tracking*

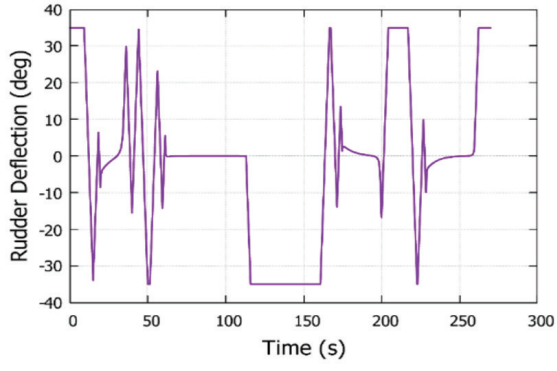

Figure 13*. Rudder deflection during the waypoint tracking*

4.2. Real-Time Simulator Design

In order to simulate the dynamics of the ship in a visual environment, an open-source flight simulator, FlightGear, is utilized. Data is transmitted to FlightGear through the utilization of the Aerospace Toolbox within MATLAB/Simulink. As shown in Figure 14, modelling and control of the ship are carried out within MATLAB/Simulink, and

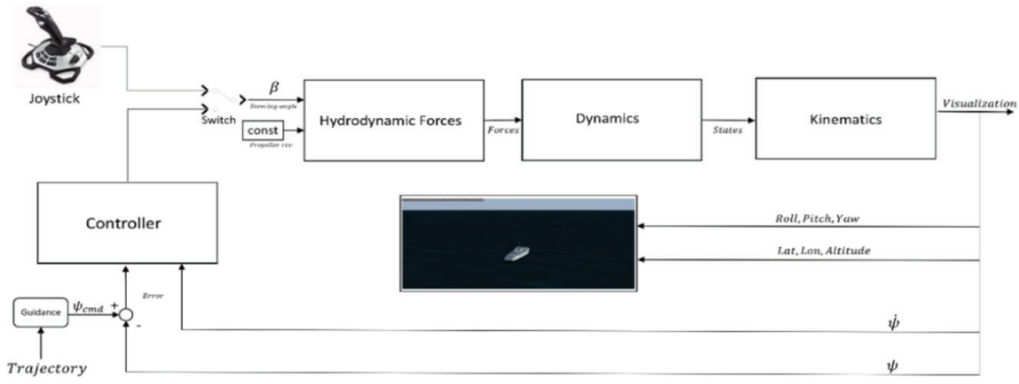

Figure 14. *Closed loop control testing: Real-time marine simulator setup*

the three degrees of freedom data is visualized through the use of the FlightGear block within the Aerospace Blockset of MATLAB/Simulink. Latitude and longitude data are given arbitrarily, whereas altitude, roll and pitch angles are kept as zero since these states are not calculated. Data transmission to FlightGear software is provided via UDP bus. This enabled the examination of the ship's behaviour in a graphical representation.

Additionally, an optional mode is incorporated into the simulation that enables switching between manual and autonomous modes during the ship's operation. The manual mode allows for the ship to be manually controlled using a joystick given in Figure 14, while the autonomous mode is executed by providing the required waypoint for the ship to navigate to. The switching between two modes is facilitated using a joystick.

5. Conclusion

In this study, autonomous trajectory tracking of a ship has been executed by using a model-based control approach. The ship's motion is modelled using dynamics, kinematics and hydrodynamic force equations, which are subsequently validated through a turning maneuver test and comparison with experimental data. To achieve autonomous control of the ship's heading angle, a cascade control structure is employed. Controller parameters are optimized using both PSO and GA optimization methods. The cost function that is required to be minimized is the combination of integral time absolute errors of both inner and outer loops. As the most important contribution of this study, a comparison has been executed between the optimization methods in terms of computational efficiency. It has been found that the PSO is faster than the GA method to find the optimal parameters that minimizes the cost function. Afterwards, a guidance algorithm is given that determines the heading angle change for corresponding waypoints. It is shown that the ship is able to track given waypoints autonomously. A real time simulator has been employed to visualize the motion of the ship in a graphical environment.

Ongoing researches on this study may consist of designing different linear/non-linear controllers and comparing the performances of different controllers; designing an observer to filter the output of the system in the presence of noise such as Kalman filter. Additionally, the simulation may be improved by different model-based design steps such as software-in-the-loop, processor-in-the-loop and hardware-in-the-loop to achieve a real-time controlled system.

Authorship Contributions

Concept Design: E. Sayin, and I. Bayezit, Data Collection or Processing: E. Sayin, Analysis or Interpretation: E. Sayin, and I. Bayezit, Literature Review: E. Sayin, and I. Bayezit, Writing, Reviewing and Editing: E. Sayin, and I. Bayezit.

Funding: The authors declare that no funds, grants, or other support was received during the preparation of this manuscript.

References

[1] P. Dash, L. C. Saikia, and N. Sinha, "Automatic generation control of multi area thermal system using bat algorithm optimized PD–PID cascade controller". *International Journal of Electrical Power & Energy Systems*, vol. 68, pp. 364-372, Jun 2015.

[2] K. S. Kula, "Heading control system with limited turning radius based on IMC structure", in *21st International Conference on Methods and Models in Automation and Robotics (MMAR),* 29 August 2016 - 01 September 2016, Miedzyzdroje, Poland [Online]. Available: IEEE Xplore, https://ieeexplore.ieee.org [Accessed: 26 Sep 2016].

[3] H. Li, and K. Wang, "The design of ship dynamic positioning controller", in *2014 Sixth International Conference on Intelligent Human-Machine Systems and Cybernetics,* 26-27 August 2014 Hangzhou, China [Online]. Available: IEEE Xplore, https://ieeexplore.ieee.org [Accessed: 09 Oct 2014].

[4] M. Tao, and F. Ma, "Research on ship control with mechanical arms based on the PID controller", in *2021 6th International Conference on Transportation Information and Safety (ICTIS),* October 2021 Wuhan, China [Online]. Available: IEEE Xplore, https://ieeexplore.ieee.org/ [Accessed: 27 Jun 2022].

[5] J. Zhibin, L. Tiejun, X. Huixi, and W. Fuli, "Diving control of autonomous underwater vehicle based on cascade control and tracking differentiator", in *OCEANS 2016-Shanghai*, 10-13 April 2016, Shanghai, China [Online]. Available: IEEE Xplore, https://ieeexplore.ieee.org/ [Accessed: 09 Jun 2016].

[6] L. Andrija, S. Vedran, and B. Juraj, "Unmanned surface vehicle-tritor". *Brodogradnja*, vol. 73, pp. 135-150, 2022.

[7] O. S. Sahin, E. Kahramanoglu, F. Cakici, and E. Pesman, "Control of dynamic trim for planing vessels with interceptors in terms of comfort and minimum drag". *Brodogradnja*, vol. 74, pp. 1-17, 2023.

[8] Z. Li, and J. Sun, "Disturbance compensating model predictive control with application to ship heading control". *IEEE Transactions on Control Systems Technology,* vol. 20, pp. 257-265, Feb 2011.

[9] T. Asfihani, K. Chotimah, and I. Fitria, "Ship heading control using nonlinear model predictive control", in *3rd International Seminar on Research of Information Technology and Intelligent Systems (ISRITI)*, 10-11 December 2020, Yogyakarta, Indonesia [Online]. Available: IEEE Xplore, https://ieeexplore.ieee.org/ [Accessed: 13 Jan 2021].

[10] S. Subchan, A. M. Syafii, T. Asfihani, and D. Adzkiya, "Modified kalman filter-based model predictive control for ship heading control with probabilistic constraints". *Systems Science & Control Engineering*, vol. 9, pp. 109-116.

[11] T. T. Le, "Ship heading control system using neural network". *Journal of Marine Science and Technology*, vol. 26, pp. 963-972, Jan 2021.

[12] D. M. Pathan, T. Hussain, J. Daudpoto, and I. A. Memon, "Neural network steering controller for a ship". *Sindh University Research Journal-SURJ (Science Series)*, vol. 44, pp. 399-404, 2012.

[13] L. P. Perera, and C. G. Soares, "Pre-filtered sliding mode control for nonlinear ship steering associated with disturbances". *Ocean Engineering*, vol. 51, pp. 49-62, Sep 2012.

[14] L. Yuan, and H. Wu, "Simulation and design of fuzzy sliding-mode controller for ship heading-tracking". *Journal of Marine Science and Application*, vol. 10, pp. 76-81, Apr 2011.

[15] H. Zhang, X. Zhang, and R. Bu, "Radial basis function neural network sliding mode control for ship path following based on position prediction". *Journal of Marine Science and Engineering*, vol. 9, 1055, 2021.

[16] X. Lu, Z. Liu, and Z. Chu, "Nonlinear adaptive heading control for an underactuated surface vessel with constrained input and sideslip angle compensation". *Brodogradnja*, vol. 71, pp. 71-87, 2020.

[17] S. Paramesh, and S. Rajendran, "A unified seakeeping and manoeuvring model with a PID controller for path following of a KVLCC2 tanker in regular waves". *Applied Ocean Research*, vol. 116, 102860, 2021.

[18] J. Adams, A. C. Dubey, and S. Rajendran, "A model predictive based controller (MPC) for the path following of a KVLCC2 tanker in waves", in *OCEANS 2022-Chennai*, 21-24 February 2022, Chennai, India [Online]. Available: IEEE Xplore, https://ieeexplore.ieee.org/ [Accessed: 19 May 2022].

[19] R. Sandeepkumar, S. Rajendran, R. Mohan, and A. Pascoal, "A unified ship manoeuvring model with a nonlinear model predictive controller for path following in regular waves". *Ocean Engineering*, vol. 243, 110165, Jan 2022.

[20] S. Wang, X. Yan, F. Ma, P. Wu, and Y. Liu, "A novel path following approach for autonomous ships based on fast marching method and deep reinforcement learning". *Ocean Engineering*, vol. 257, 111495, Aug 2022.

[21] H. Yasukawa, and Y. Yoshimura, "Introduction of MMG standard method for ship maneuvering predictions". *Journal of Marine Science and Technology*, vol. 20, 37-52, 2015.

[22] T. Perez, and T. I. Fossen, "Ship motion control: kinematics of ship motion". *Springer*, pp. 45-58, Trondheim, Norway, 2005.

[23] O. K. Kinaci, I. Bayezit, and M. Reyhanoglu, "A practical feedforward speed control system for autonomous underwater vehicles". *Ocean Engineering*, vol. 218, 108214, Dec 2020.

[24] O. K. Kinaci, M. K. Gokce, A. D. Alkan, and A. Kukner, "On self-propulsion assessment of marine vehicles". *Brodogradnja*, vol. 69, pp. 29-51, 2018.

[25] A. C. Dimian, C. S. Bildea, and A. A. Kiss, "Chapter 15 - plantwide control". *Computer Aided Chemical Engineering,* vol. 35, pp. 599-647, 2014.

[26] S. Kumar, S. Jain, and H. Sharma, Advances in swarm intelligence for optimizing problems in computer science, *Chap. 2. Chapman and Hall/CRC, New York, USA*, 27-52, 2018.

[27] I. Bayezit, R. Bitirgen, M. Hançer, and O. K. Kinaci, "Strait of Istanbul crossing simulation of a VLCC type ship in autopilot mode". *Journal of ETA Maritime Science*, vol. 7, pp. 304-316, Dec 2019.

[28] D. Maiti, A. Acharya, M. Chakraborty, A. Konar, and R. Janarthanan, "Tuning PID and PIλ Dμ controllers using the integral time absolute error criteria", in *4th International Conference on Information and Automation for Sustainability ICIAFS*, 12-14 December 2008, Colombo, Sri Lanka [Online]. Available: IEEE Xplore, https://ieeexplore.ieee.org [Accessed: 13 Feb 2009].

[29] M. V. Sadasivarao, and M. Chidambaram, "PID Controller tuning of cascade control systems". *Journal of the Indian Institute of Science*, vol. 86, pp. 343-354, Jul-Aug 2006.

[30] O. Kramer, Genetic Algorithms. In: Genetic Algorithm Essentials. Studies in Computational Intelligence, Springer, Cham. 2017, pp. 11-19.

[31] S. Katoch, S. S. Chauhan, and V. Kumar, "A review on genetic algorithm: past, present, and future". *Multimedya Tools and Applications*, vol. 80, pp. 8091-8126, 2021.

[32] A. Lambora, K. Gupta, and K. Chopra, "Genetic algorithm-a literature review", in *International Conference on Machine Learning, Big Data, Cloud and Parallel Computing (COMITCon)*, 14-16 February 2019, Faridabad, India. [Online]. Available: IEEE Xplore, https://ieeexplore.ieee.org [Accessed: 11 Oct 2019].

[33] R. Poli, J. Kennedy, and T. Blackwell, "Particle swarm optimization". *Swarm Intelligence*, vol. 1, pp. 33-57, Aug 2007.

[34] T. Dlabač, M. Ćalasan, M. Krčum, and N. Marvučić, "PSO-based PID controller design for ship course-keeping autopilot". *Brodogradnja*, vol. 70, pp. 1-15, 2019.

[35] F. Marini, and B. Walczak, "Particle swarm optimization (PSO). A tutorial". *Chemometrics and Intelligent Laboratory Systems*, vol. 149, pp. 153-165, Dec 2015.

[36] A. P. Piotrowski, J. J. Napiorkowski, and A. E. Piotrowska, "Population size in particle swarm optimization". *Swarm and Evolutionary Computation*, vol. 58, 100718, Nov 2020.

[37] T. I. Fossen, *Marine Control Systems: Guidance. Navigation, and Control of Ships, Rigs and Underwater Vehicles*, Marine Cybernetics, Trondheim, Norway, 2002.